Temporal and spectral correlation of acoustic and chemiluminescent signal of a liquid-fueled turbulent swirl burner

Gy. Hidegh*, V. Józsa

Department of Energy Engineering, Faculty of Mechanical Engineering, Budapest University of Technology and Economics, H-1111 Budapest, Műegyetem rkp. 3

Abstract

Real-time diagnostics and control of modern combustion chambers are required in order to fulfill pollutant emission standards and ensure high-efficiency operation. If the acoustic disturbances are in phase with heat release disturbances, the resulting fluctuation will have positive feedback and lead to combustion failure or structural damage. Presently, combustion in a 15 kW liquid fueled burner was analyzed by using a microphone and a photomultiplier tube. The synchronously acquired data were evaluated by two spectral techniques, Fast Fourier Transform, and Continuous Wavelet Transform. Finally, the temporal signal is analyzed by correlation functions at several window sizes. The comparison of the spectral data of the two sensors showed no correlation, unlike the temporal data.

Introduction

Combustion chambers feature lean combustion in several modern applications to ensure low emissions and high efficiency [1]. However, such an operation may lead to combustion failure or even structural damage if the heat release and acoustic fluctuations show positive feedback [2]. In order to prevent these situations, active [3] and passive [4] elements can be used. The problem persists for all combustion applications independent of the fuel type, composition, and phase. However, the injection, evaporation, and mixing affect the process. Nowadays, the applications demand wide operating regime with continuous maneuvering capability. Therefore, combustion chamber control algorithms need to operate adaptively [5] to eliminate most of the effects which are not tested during the evaluation phase.

The phase of the chemiluminescent and acoustic signals can be calculated by using the Rayleigh criterion, defined by Eq. (1):

$$R = \int_0^\tau q(t)p(t)\mathrm{d}t, \qquad (1)$$

where q is the heat release rate, and p is the fluctuating pressure, both as a function of the time, t. R is the Rayleigh index which is positive if the heat release rate and the pressure fluctuations are in phase, leading to instabilities. Zero means that the two signals are not correlated while a negative correlation means dampening of the fluctuation amplitudes. Non-premixed, swirling propane flames were investigated by Idahosa et al. [6] under non-forced and forced conditions up to 315 Hz since the low-frequency components of V-shaped flames are located below this value, which was excited. Zhou et al. [7] also investigated a non-premixed, swirl-stabilized flame with side excitation to model the effect of cross-flow perturbation on flame characteristics.

Even though the coupling of heat release and pressure fluctuations play an emphasized role in combustion instabilities, it should be noted that entropy waves [8] may couple with either of the mentioned signals which will be followed by the other signal which was intact initially. In addition, the acoustic energy losses are not considered in the definition of the Rayleigh criterion. Similarly, it does not include the effects of other instability driving mechanisms, like equivalence ratio or swirl number fluctuation [9].

The acoustic data is sensed by a microphone since all fluid dynamics-related perturbation causes a disturbance in the pressure field. Therefore, the propagation of the pressure waves is straightforward to sense. However, the sensing of the chemiluminescent signal requires further considerations. Firstly, the range of time scales of the chemical reactions exceeds that of the fluid dynamics in both directions by a few magnitudes [10]. The chemiluminescent signal of premixed hydrocarbon flames is characterized by OH* and CH* which both follow the heat release rate well [11]. Typically, researchers use filters to follow either of the excited radicals at 310 nm and 430 nm for OH* and CH*, respectively [12]. It should be considered that a narrow-band filter absorbs a significant portion of the signal [13]. The use of either OH* or CH* is common in the literature. Mejia et al. [14] used a CH* filter for stability analysis of a methane-fueled slot burner. Similarly, Khalil and Gupta [15] also used CH* filter for a methane-fueled, swirl burner with O_2 and CO_2 dilution. Muruganandam et al. [3] used OH* filter for a swirl burner using premixed methane-air. Guyot et al. [13] showed that there is < 20% deviation from the average OH*/CH* ratio across the flame of a turbulent premixed industrial swirl burner fueled by methane.

The literature is rich in the investigation of stability analysis of various burner configurations utilizing mostly methane. However, it was shown earlier in the presently used test rig, which is detailed in the following section, that liquid-fueled burners might show different spectral characteristics [16]. Consequently, this paper focuses on the comparison of the temporal signal recorded by a microphone and a photomultiplier tube (PMT) and its correlation in the spectral space. The analysis is performed without acoustical excitation.

* Corresponding author: hidegh@energia.bme.hu

Measurement setup

The investigated atmospheric test rig is shown in **Fig. 1**. The combustion air flow rate, delivered by the fan into the preheater, was controlled by a frequency inverter, and therefore, it controlled the air-to-fuel equivalence ratio, λ. The combustion air was preheated to 400 °C with electrical heaters to enhance the vaporization of the liquid fuel droplets. The test rig was designed for 15 kW combustion power, thus the mass flow of the applied standard diesel oil (EN 590:2014) was constant over the course of the measurements. More details on the test equipment can be found in the literature [17,18].

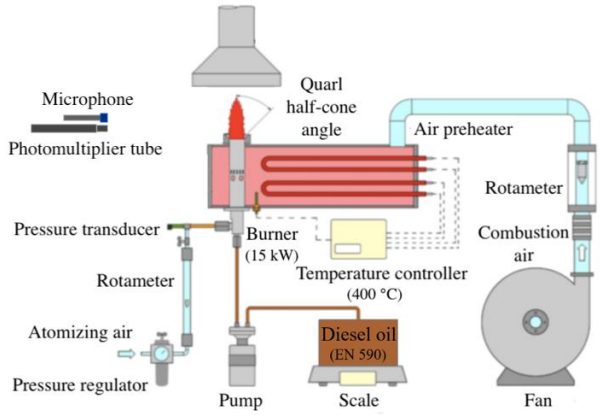

Fig. 1. Atmospheric test rig.

The investigated turbulent lean premixed prevaporized (LPP) swirl burner is shown in **Fig. 2**. It was originally operated in a Capstone C-30 micro gas turbine. The length of the mixing tube is 75.5 mm, and its inner diameter is 26.8 mm. On the mixing tube, there are fifteen rectangular holes with a 45° inlet angle to swirl the combustion air, and four other circular inlets to prevent flashback. The lip of the burner was equipped with a 45° half-cone angle quarl in order to have better flame stability.

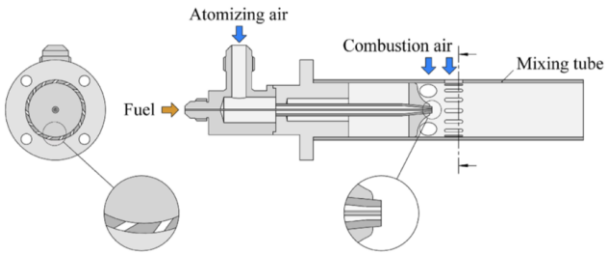

Fig. 2. Investigated LPP burner.

The burner features a plain-jet airblast atomizer in which the annular air flow blows over the liquid jet at few hundred m/s velocity difference. The resulting interaction leads to the disruption of the jet into tiny droplets. During the measurements, three atomizing gauge pressures, p_g, and three λs were set; the resulting measurement setup matrix is shown in **Table 1**.

Table 1. The measurement setups.

p_g [bar$_g$] \ λ [-]	1	1.12	1.24
0.3	Case 1	Case 2	Case 3
0.5	Case 4	Case 5	Case 6
0.8	Case 7	Case 8	Case 9

The chemiluminescence measurements were carried out with an optical receiver module manufactured by SMETEC GmbH, featuring a PMT. The acoustic signal was detected by a GRAS 146AE 1/2" CCP Free-field Microphone Set. Both signals were recorded synchronously by a DT9837B type dynamic signal analyzer at 2.8 kHz to focus on the sub-1 kHz spectral regime [2]. Both devices were placed in the plane of the diffuser lip, at a distance of 0.5 m from the burner. The sampling time was 26 s in each case. The recorded data of the used PMT was compared to a model 77346 PMT manufactured by Oriel Instruments. The latter PMT was equipped with an OH* filter with 302 nm center wavelength with 5 nm bandwidth and ≥ 25% transmission. The excellent correlation of the two signals (not shown here) showed that the application of the OH* filter for the measurement of the fluctuations of the heat release rate is not necessary. Therefore, the measurements were carried out with the SME Photodetec module without an OH* filter. This decision was supported by a spectrometer measurement performed earlier under the same conditions [19,20]. A spectrum in the range of 260-580 nm is shown in **Fig. 3**, where the operating conditions were the same as for Case 9. The spectral characteristics were corrected to the sensitivity of the spectrometer. It can be concluded that the chemiluminescent signal is dominated by the OH* and CH* signals, therefore, omitting the filter is appropriate from a practical point of view.

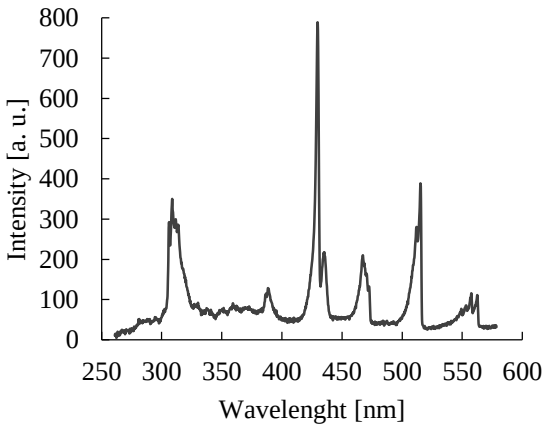

Fig. 3. The corrected flame spectrum of Case 9.

Methods

Firstly, the correlation between the acoustic and chemiluminescence signals was evaluated focusing on the spectral space, using both Fourier and Wavelet transformations. The analyzed window sizes were $w = 2^8$, 2^{10} and 2^{12}. Spectrograms were created by using short-time Fourier transform for each setup and both measurement devices. As another spectrum analyzing method, continuous 1-D wavelet transform (CWT), and wavelet coherence evaluation was performed.

Secondly, the similarity of various cuts of a single data set was analyzed in temporal space, focusing on the correlation between the signals. The raw data was normalized with respect to the mean value and the absolute maximum value. The statistical analysis was extended to probability density function (PDF) fitting. The evaluation was done by using $w = 2^9$, 2^{10}, 2^{11}, and 2^{12}.

Results and discussion

Figure 4 shows the results of the spectrum analysis of the PMT signal of Case 2, using a 2^8 window. There are no observable spectral peaks in the spectrogram and the scalogram. Nevertheless, temporal spikes are present which originate from bursts.

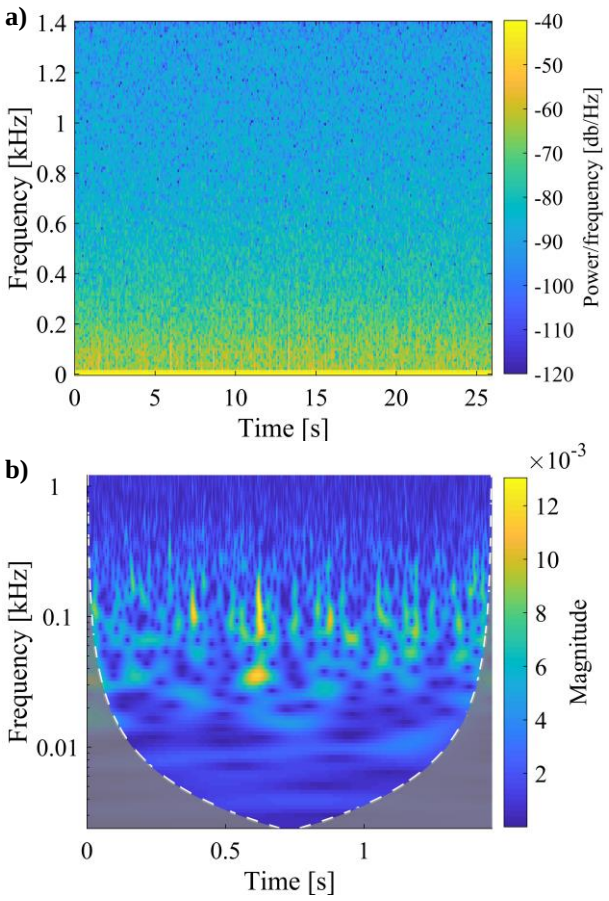

Fig. 4. a) Spectrogram, **b)** Scalogram of the PMT signal, Case 2, $w = 2^8$.

The bursts are highlighted in the scalogram where the width of these peaks decreases with the increasing frequency which originates from the multiresolution nature of the CWT. Consequently, the PMT signal is free from characteristic harmonic components.

Figure 5 shows the results of the spectrum analysis of the microphone signal of Case 2, using a 2^8 window size. The majority of the energy content in the range of 0-1.4 kHz is concentrated in the 200-400 Hz regime. However, there is no outstanding peak as combustion is a broadband phenomenon [21]. The intermittency of the spectrum is clearly visible in both the spectrogram and the scalogram. The counterparts of the bursts mentioned in **Fig. 4**, were not located in either plot.

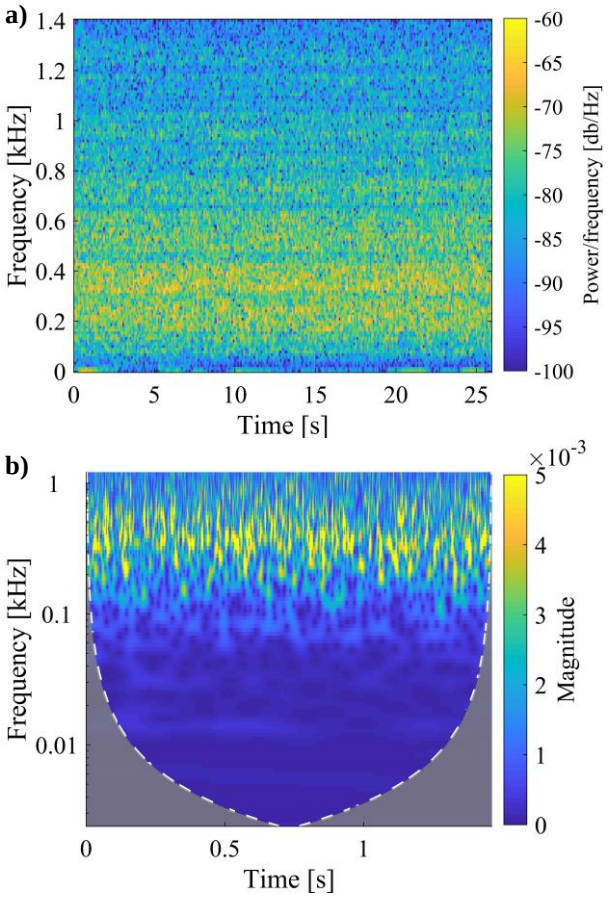

Fig. 5. a) Spectrogram, **b)** Scalogram of the microphone, Case 2, $w = 2^8$.

Figure 6 shows the comparison of the CWTs of **Figs. 4b** and **5b** PMT using wavelet coherence. Since the majority of the correlating part of the two signals is concentrated below 125 Hz, which regime plays a negligible role, it can be stated that the two signals are not well-correlated in the spectral space. The above analysis was performed for various slices from the 26 s recorded data, and the effect of w, p_g, and λ was also evaluated. However, the results did not change notably, the characteristics were similar for each case as the presented ones above. This conclusion is supported by Idahosa et al. [6] indirectly since the amplitude of the

signal varied for different Rayleigh indices, but no evident peak was found in the CH* signal. More recently, Rock et al. [22] used an empirically derived method to capture the precursors of lean blowout using the temporal signal. Therefore, the following part will discuss the results of the temporal signal analysis.

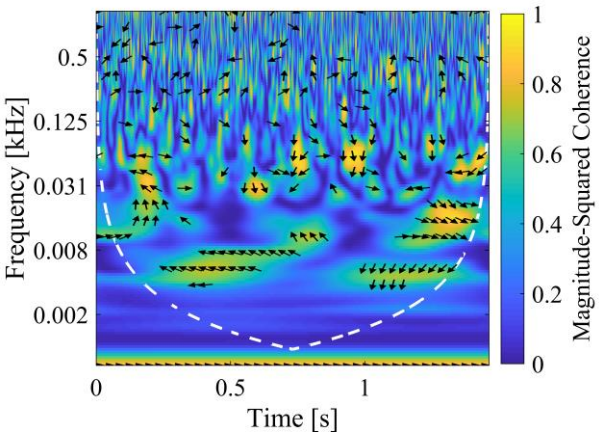

Fig. 6. Wavelet coherence of the PMT and the microphone signal, Case 2, $w = 2^8$.

The correlation coefficients of the normalized data of the PMT and microphone signals are shown in **Fig. 7**. The size of the applied window does not affect the mean values; however, the standard deviation is increasing as the signal is divided into more segments due to the intermittency that is previously noted in the spectral analysis. Consequently, it is not a trivial choice what sample size should be analyzed of the temporal signal. A weak linear correlation of the two data sets can be seen as it was expected since no stability limit was approached. Consequently, the correlation between the two signals exists, however, not consisting of harmonics.

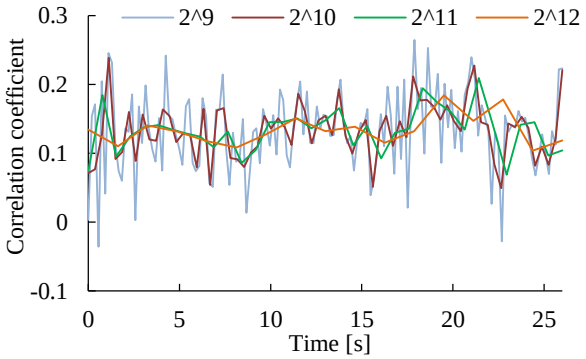

Fig. 7. Correlation coefficients of the normalized data of the PMT and the microphone.

The correlation of the normalized signals of the two devices was evaluated focusing on the mean values and standard deviation of the correlation coefficients of the data sets measured by the PMT and the microphone. The former is presented for $w = 2^{10}$ in **Fig. 8**, with respect to the nine measurement setup cases. Note that the results were closely identical for all other windows sizes. The mean value is increasing with λ while its standard deviation was practically negligible (O(1E-16)).

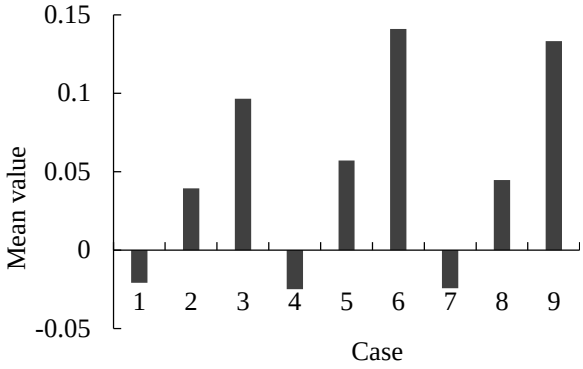

Fig. 8. Mean values of the correlation coefficients of the data sets of the PMT and the microphone, $w = 2^{10}$.

The similarity of the data sets recorded by the same sensor was analyzed by probability density function (PDF) fitting. By evaluating widely used PDFs, the microphone and the PMT data followed Normal (N) and Generalized Extreme Value (GEV) distributions, respectively. **Figure 9** shows the fitted PDFs of Case 9 for the whole 26 s signal.

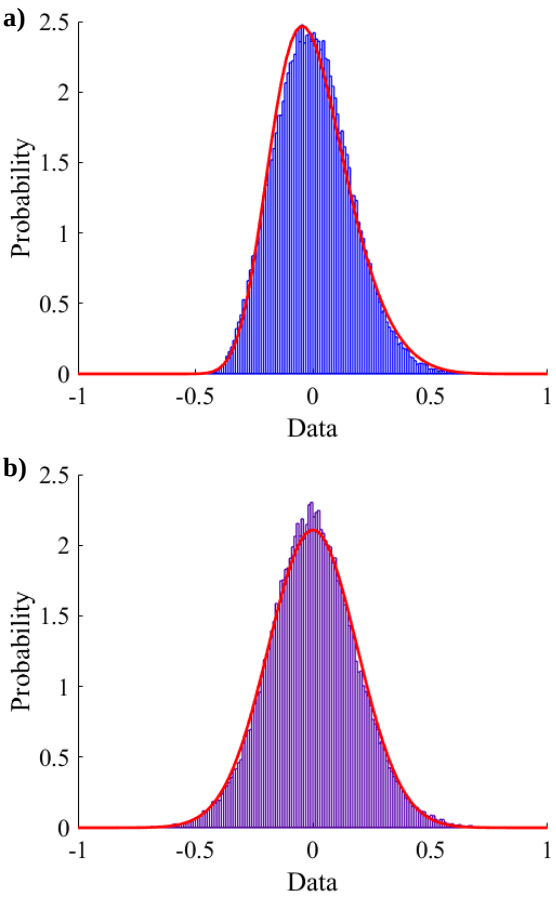

Fig. 9. a) GEV distribution fitted on the data of the PMT, **b)** N distribution fitted on the data of the microphone, Case 9.

In the present case, the correlation of parameters of two distributions can be compared. GEV has shape, scale, and location parameters while N has only scale and location parameters. Since the microphone signal oscillates around zero, the location parameter of the fitted PDF does not vary. Hence, the correlation of the scale parameters was evaluated which refers to the spread of the PDF. The results are presented in **Fig. 10** for $w = 2^{10}$. Note that the result is depending on the size of w, however, follow a similar trend for $w = 2^9$ and 2^{10}. Consequently, the window size is a crucial point for data evaluation. Local disturbances are averaged by the large windows, however, a short window might show an extreme scatter where the trends are difficult to follow.

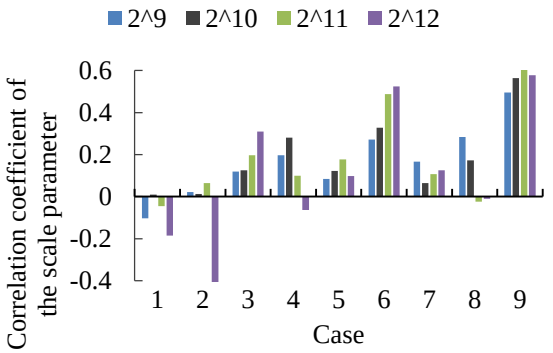

Fig. 10. Correlation coefficients of the scale parameters with varying w.

Finding the most suitable PDF for a given data set was performed by calculating the log-likelihood values. Nevertheless, this is also depending on the data set, hence, on w and time. **Figure 11** shows the log-likelihood values of the PDFs related to the segments of the data set of Case 3, applying $w = 2^{10}$.

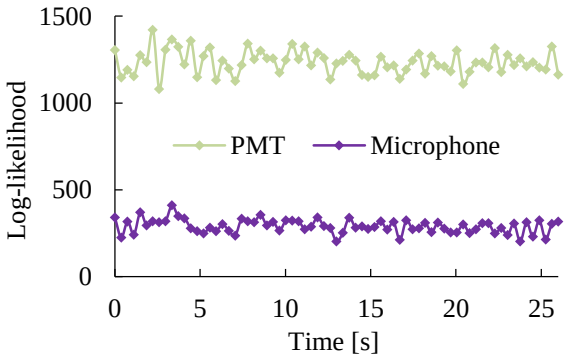

Fig. 11. Log-likelihood values of the fitted PDFs on the data of the PMT and the microphone, Case 3, $w = 2^{10}$.

Figure 12 shows the relative standard deviation of the log-likelihood at $w = 2^{10}$ for the nine cases. As the applied window size decreased, the relative standard deviation of the log-likelihood increased, following the trend of **Fig. 7**. Among the two signals, the log-likelihood of the microphone data was characterized by a larger relative standard deviation which was also observed in **Fig. 11**. However, the N PDF showed the best fit among several other PDFs; it does not describe the ongoing physical phenomena fully. This result was probably supported by the central limit theorem, namely, the sum of several non-normal PDFs with finite expected value and variance gives a normal distribution even though the subprocesses follow a different PDF. Nevertheless, the GEV characterizes the PMT signal fairly in all cases.

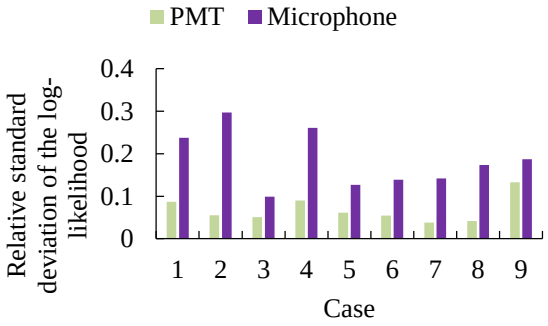

Fig. 12. The relative standard deviation of the log-likelihood at $w = 2^{10}$ for the nine cases.

Conclusions

In the present paper, chemiluminescent and the acoustic signal of a 15 kW swirl burner fueled with standard diesel oil was investigated without acoustical excitation. Through the control of the combustion air flow rate and the atomizing gauge pressure, nine operating points were set. Spectral and temporal analysis of the microphone and photomultiplier tube data sets was carried out. The following conclusions were derived:

- Through Fourier and Wavelet transformations the comparison of the two signal was not effective; the coherence of two spectra was low. The PMT spectrum showed temporal burst rather than consequent peaks in a frequency band like the microphone data.
- The signal length has a considerable effect on the temporal signal due to intermittency. Hence, the mean value does not vary unlike the standard deviation of the correlation coefficients. The resulting low correlation between the PMT and microphone signal is the result of the stable operation.
- By fitting PDFs, the Generalized Extreme Value function provided the best fit for the PMT signal while Normal distribution suited the microphone signal the best. Nevertheless, the high relative standard deviation of the comparable scale parameter showed that the latter choice was less adequate than the former PDF for the PMT data.

Acknowledgments

This paper was supported by the National Research, Development and Innovation Fund of Hungary, project №. OTKA-FK 124704, New National Excellence Program of the Ministry of Human Capacities project №.

ÚNKP-18-4-BME-195, Artificial Intelligence research area of Budapest University of Technology and Economics (BME FIKP-MI), and the János Bolyai Research Scholarship of the Hungarian Academy of Sciences.

References

[1] Lefebvre AH, Ballal DR. Gas turbine combustion. third. Boca Raton: CRC Press; 2010.

[2] Huang Y, Yang V. Dynamics and stability of lean-premixed swirl-stabilized combustion. Prog Energy Combust Sci 2009;35:293–364. doi:10.1016/j.pecs.2009.01.002.

[3] Muruganandam TM, Nair S, Scarborough D, Neumeier Y, Jagoda J, Lieuwen T, et al. Active Control of Lean Blowout for Turbine Engine Combustors. J Propuls Power 2005;21:807–14. doi:10.2514/1.7254.

[4] Yadav NP, Kushari A. Passive control of premixed lifted flame in a dump combustor. Fuel 2012;93:67–74. doi:10.1016/j.fuel.2011.09.010.

[5] Evesque S. Adaptive Control of Combustion Oscillations. Control 2000:182.

[6] Idahosa U, Saha A, Xu C, Basu S. Non-premixed acoustically perturbed swirling flame dynamics. Combust Flame 2010;157:1800–14. doi:10.1016/j.combustflame.2010.05.008.

[7] Zhou H, Huang Y, Meng S. Response of non-premixed swirl-stabilized flames to acoustic excitation and jet in cross-flow perturbations. Exp Therm Fluid Sci 2017;82:124–35. doi:10.1016/j.expthermflusci.2016.11.007.

[8] Nicoud F, Poinsot T. Thermoacoustic instabilities: Should the Rayleigh criterion be extended to include entropy changes? Combust Flame 2005;142:153–9. doi:10.1016/j.combustflame.2005.02.013.

[9] Kim KT. Combustion instability feedback mechanisms in a lean-premixed swirl-stabilized combustor. Combust Flame 2016;171:137–51. doi:10.1016/j.combustflame.2016.06.003.

[10] Maas U, Pope SB. Simplifying chemical kinetics: Intrinsic low-dimensional manifolds in composition space. Combust Flame 1992;88:239–64. doi:10.1016/0010-2180(92)90034-M.

[11] Panoutsos CS, Hardalupas Y, Taylor AMKPMKP. Numerical evaluation of equivalence ratio measurement using OH* and CH* chemiluminescence in premixed and non-premixed methane-air flames. Combust Flame 2009;156:273–91. doi:10.1016/j.combustflame.2008.11.008.

[12] Gaydon AG. The spectroscopy of flames. 2nd ed. Chapman and Hall Ltd., London; 1974. doi:10.1016/0010-2180(75)90098-X.

[13] Guyot D, Guethe F, Schuermans B, Lacarelle A, Paschereit CO. CH*/OH* Chemiluminescence response of an atmospheric premixed flame under varying operating conditions. Proccedings ASME Turbo EXPO 2010:1–12. doi:http://dx.doi.org/10.1115/GT2010-23135.

[14] Mejia D, Miguel-Brebion M, Selle L. On the experimental determination of growth and damping rates for combustion instabilities. Combust Flame 2016;169:287–96. doi:10.1016/j.combustflame.2016.05.004.

[15] Khalil AEE, Gupta AK. Acoustic and heat release signatures for swirl assisted distributed combustion. Appl Energy 2017;193:125–38. doi:10.1016/j.apenergy.2017.02.030.

[16] Józsa V, Kun-balog A, Józsa V. Spectroscopic analysis of crude rapeseed oil flame. Fuel Process Technol 2015;139:61–6. doi:10.1016/j.fuproc.2015.08.011.

[17] Józsa V, Kun-Balog A. Stability and emission analysis of crude rapeseed oil combustion. Fuel Process Technol 2017;156:204–10. doi:10.1016/j.fuproc.2016.11.004.

[18] Józsa V, Kun-Balog A. Effect of diffusers on the blowout stability and emission of pollutants of a liquid fueled swirl burner. J Eng Gas Turbines Power 2018. doi:10.1115/1.4039056.

[19] Józsa V, Sztankó K. Flame Emission Spectroscopy Measurement of a Steam Blast and Air Blast Burner. Therm Sci 2017;21:1021–30.

[20] Hidegh G, Józsa V. Correlation of chemiluminescent signal and pollutant emission of a liquid-fueled turbulent swirl burner. Conf. Proc. 1st Int. Conf. Smart Energy Carriers, 2019, p. 3–6.

[21] Reed RJ. North American Combustion Handbook, vol. 2. third. Cleveland, OH: North American Mfg. Co.; 1997.

[22] Rock N, Emerson BL, Seitzman J, Lieuwen T. Dynamics of Spray Flames under Near-Lean Blowoff Conditions. Proc. AIAA Scitech 2019 Forum, 2019, p. 1–16. doi:10.2514/6.2019-1433.